Synthetic model microswimmers near walls

Ketzetzi, S.

2

Wall-Dependent Propulsion Speeds

Abstract

Catalytic model microswimmers that propel due to self-generated fluid flows exhibit strong affinity for surfaces. In this chapter, we measure the speed of catalytic microswimmers near planar walls (substrates) and report a significant dependence of their speeds on the substrate material. We find that speed scales with the solution contact angle on the substrate, which relates to the associated hydrodynamic substrate slip length. We show that such speed dependence can be attributed to osmotic coupling between swimmers and substrate. Our work therefore points out that hydrodynamic slip at nearby walls, though often unconsidered, can impact self-propulsion.

The text in this chapter is based on:

S. Ketzetzi, J. de Graaf, R. P. Doherty, D. J. Kraft, Phys. Rev. Lett. 124, 048002 (2020), "*Slip Length Dependent Propulsion Speed of Catalytic Colloidal Swimmers near Walls*"; doi: 10.1103/PhysRevLett.124.048002

Introduction

Colloidal swimmers constitute a new class of nonequilibrium model systems that also hold great promise for applications owing to their fast directed motion in liquid environments. A simple experimental realization of such microswimmers are spherical colloids half coated with Pt [54]. These colloids move autonomously in H_2O_2 solutions due to asymmetric catalytic reactions taking place on their surfaces [42] and are typically found self-propelling parallel to a substrate [59, 60, 75, 94]. This substrate affinity leads to accumulation [75] and retention [59–61] of swimmers at surfaces, such as walls and obstacles, and can be exploited as a means to guide their motion [59, 95].

Strikingly, upon approaching a surface, numerical and theoretical models predict both an increase or decrease in swimming speed depending on the considered propulsion mechanism and the physicochemical properties of the swimmer and wall [96–102]. At the same time, experimental observations also hint at non-negligible substrate effects on the speed of synthetic swimmers [103–105]. In fact, substrate effects may be at the heart of inconsistencies in catalytic microswimmer speeds under comparable experimental conditions. For example, speeds as disparate as 18 μm/s [75] and 3 μm/s [30] were found for polystyrene spheres with 5 nm Pt coating in 10% H_2O_2. This difference is even more surprising when one considers that the slower speeds were observed for the smaller species, whereas the speed of Pt-coated swimmers should scale inversely with size [58].

Recent measurements on different polymer-coated substrates revealed a propulsion speed decrease upon functionalization with either positively or negatively charged polyelectrolytes for bimetallic swimmers [103]. This is puzzling because contrary to most current predictions it indicates that the wall zeta potential does not have a dominant effect on the speed of self-electrophoretic swimmers. Furthermore, photoactivated TiO_2/SiO_2 swimmers were found to swim with 3 μm/s speed on glass, while they propelled with 4 μm/s speed on gold (Au) coated glass substrates [105]. It was proposed, based on zeta potential values for Au and glass at neutral pH conditions, that the increase in the propulsion speed stemmed from the lower zeta potential of the Au surface. However, neutral conditions are likely not met in H_2O_2 solutions. Even more so, results obtained using Au-coated substrates are hard to

interpret, because Au could in principle catalyze H_2O_2 decomposition and therefore interfere with the propulsion reaction [105]. To elucidate the origin of these intriguing observations, other surfaces ought to be examined in a quantitative manner. Understanding potential surface effects on colloid self-propulsion is essential not only for their use as model systems and the development of a quantitative framework but also for future applications that may require motion in complex environments comprising obstacles or confining walls [106].

In this chapter, we quantitatively examine the effect of various substrates, namely glass, glass coated with the organosilicon compound polydimethylsiloxane (PDMS), and plastic substrates made of a polyethylene (PE) or polystyrene (PS) derivative, on the speed of catalytic colloidal swimmers. Under otherwise fixed conditions, we observe significant differences in propulsion speeds, which cannot be fully accounted for by the substrate zeta potential. Instead, we find that speeds upon different substrates fall on a single curve as a function of the solution-substrate contact angle which relates to the substrate slip length [107]. After careful examination of the observed dependence in view of qualitative and scaling arguments, and accounting for possible couplings between swimmers and the substrate, we show that substrate-dependent speeds may result from osmotic coupling.

Results and Discussion

For all experiments, we used 2.7 μm diameter TPM colloids [108] half-coated with 4.9 nm of Pt by sputter-coating, see inset in Figure 2.1 with the brighter hemisphere indicating the coating. Colloids were prepared in one batch, hence any inhomogeneities arising from their preparation, including Pt thickness that affects H_2O_2 decomposition, should be universal. Measurements were taken in the dark typically within the hour after dispersing the colloids at dilute particle concentration in deionized water con-

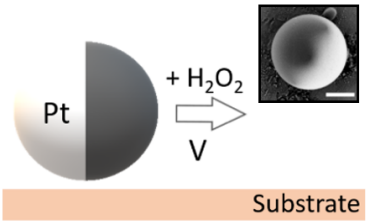

Figure 2.1: **Schematic of the experiment**. The self-propulsion of Pt-coated colloids was observed above various substrates under fixed conditions; the inset shows a SEM image of a representative colloid (scale bar is 1 µm).

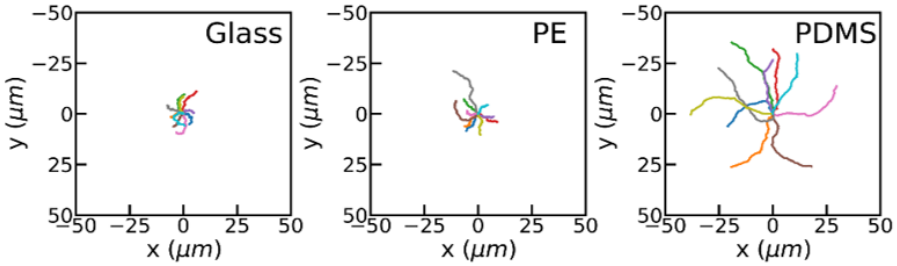

Figure 2.2: **Influence of the substrate on colloid self-propulsion.** Typical 8 s active colloid trajectories on glass, PE and PDMS.

taining 10% H_2O_2. The colloids quickly reached the lower surface and continued to self-propel parallel to it, as in Figure 2.1. Figure 2.2 shows 10 representative xy trajectories on glass, PE, and PDMS substrates acquired over a time interval of 8 s. We find that the colloids cover significantly greater distances on PDMS than on glass and PE, clearly demonstrating that the substrate affects colloid motion.

To quantify the differences in the observed behavior, we first obtain the speed V of each individual colloid from its short-term mean squared displacement following Ref. [30]. We fit the corresponding probability density function (PDF) of the speed with a log-normal distribution following Ref. [109] to obtain the speed distribution parameters on each substrate. The most frequently encountered speeds, as obtained from the fitted peak position of each PDF, are 1.05 ± 0.09, 1 ± 0.2, and 2.8 ± 0.3 μm/s, above glass, PE, and PDMS, respectively. Interestingly, though all three substrates are chemically different, the colloids show similar speeds for two of the substrates and a notably different speed for the third. At the same time, the characteristic time scale for rotation τ_R [30, 83, 110] is similar for all three substrates. Details on the determination of V and τ_R can be found in the Methods. In the absence of H_2O_2, however, the translational diffusion coefficients are similar, namely 0.099 ± 0.005, 0.098 ± 0.008, and 0.105 ± 0.005 $\mu m^2/s$, for glass, PE and PDMS, respectively. Thus, substrate-dependent differences arise only in the active state.

While speeds may be influenced by colloid properties, such as size [58], roughness [57] and slip [56, 111], these effects are negligible here since the same colloid batch was used in all experiments. Therefore, the observed

speed differences arise from differences in the substrate properties. To quantitatively unravel the origin of our observations, we consider substrate properties that may influence colloid motion. The fluid flow generated by the anisotropic catalytic reaction on the swimmer surface [112], and hence the swimmer's propulsion speed [63], has been predicted to be affected by the swimmer-wall distance [96–102], wall zeta potential [98, 105] and wall surface inhomogeneities [105]. Surprisingly, little consideration has been given until now on whether slip on the substrate impacts propulsion speeds, even though slip on the colloid has already been shown to do so [56]. Considering that hydrodynamic attraction in the active state pulls the colloids close to surfaces, to the extent that they even propel along the top of their container [75], colloid-substrate distances are expected to be small. Pt-coated swimmers of 2.5 μm radius have been found to not swim over 200 nm steps [60], and other experiments pointed out that distances may even be of the order of tens of nm [113, 114]. Since wall slip lengths ranging from several [115–118] to hundreds [119, 120] of nanometers and even micrometers [121] have been reported, boundary conditions could strongly affect the speed. Following Ref. [111], we hypothesize that deviations from the no-slip condition on the substrate enhance nearby swimmer's speeds. Surface slip relates to liquid-solid in-

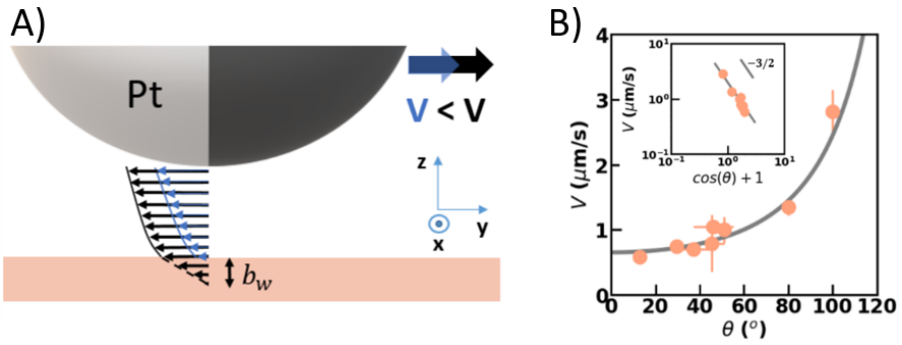

Figure 2.3: **Propulsion speed V of catalytic swimmers above substrates with different contact angle θ.** A) Schematic of the proposed model. At a given separation, the speed resulting from the colloid-generated fluid flow is larger on a hydrophobic substrate due to the larger slip length b_w (not to scale). Here, only the fluid flow velocity profile due to hydrodynamic slip on the wall is illustrated. B) V as a function of θ and least squares fit with $V = A(\cos\theta+1)^{-3/2}$ that follows from our model. The inset shows the data on a log-log scale.

teractions and thus surface wetting properties, and generally, though not always, increases with increasing hydrophobicity and thus contact angle θ [107, 117, 118, 122]. Since hydrophobic surfaces possess a larger slip fluid velocity [123], we hypothesize that they also lead to a higher propulsion speed. Conversely, the no-slip approximation on hydrophilic surfaces would lead to lower speeds, see Figure 2.3A. Indeed, the advancing contact angle measured for the H_2O_2 solution by the sessile drop method agrees with this hypothesis: θ is 46 ($\pm$ 9)^o, 51 ($\pm$ 3)^o, and 100 ($\pm$ 3)^o, for glass, PE, and PDMS (as in [124]), respectively. PE is normally hydrophobic, thus a modification has been performed by the supplier.

To further test this hypothesis, we modulated the hydrophilicity of the employed substrates and repeated the experiments. We increased the hydrophilicity of glass by either a cleaning procedure ($\theta = 29.5 \pm 3^o$) or treatment with HCl [125] ($\theta = 13 \pm 3^o$) and we observed a concomitant speed decrease by 30% and 45%, respectively. Conversely, when we rendered the glass more hydrophobic ($\theta = 80 \pm 2^o$), we found that speed increased by 28% compared to untreated glass. Similar behavior was seen on PDMS that was rendered hydrophilic through UV-ozone treatment [126, 127] ($\theta = 37 \pm 7^o$): colloids propelled four times slower than on hydrophobic PDMS. Finally, we employed commercially available hydrophilic PS substrates ($\theta = 46 \pm 6^o$) and found $V = 0.8 \pm 0.45 \mu$m/s. We summarize these findings by plotting V as a function of θ in Figure 2.3B. The collapse of the data onto a single curve suggests that θ is the most relevant parameter while other differences among substrates, besides their effect on θ, are of lesser importance.

Next, we develop a quantitative framework for the slip-dependent propulsion speeds. For our analysis we consider that the height above the substrate remains relatively unaffected by the change of substrate, as supported by our experimental measurements of the diffusion coefficient [128–130], see both experimental details in the Methods and theoretical considerations in the Appendix. When the height is left unperturbed by varying $\cos\theta$, the dominant source of change to the propulsion speed comes from solute gradients near the substrate. As mentioned earlier, these are generated by reactions taking place on the swimmer surface and, similar to the way they cause self-propulsion, lead to an effective surface fluid velocity along the wall [63], often referred to as 'slip' velocity. This effective surface fluid velocity couples back to the

swimmer, modifying its net velocity [59, 95, 98, 131]. In the Appendix, we show that neither purely hydrodynamic coupling [102, 132, 133], solute confinement [96, 97, 99–101], nor reaction-based coupling [58] can account for the significant wall effect. Instead, our observation can be attributed to osmotic coupling [59, 63, 95, 98, 131, 134]. The osmotic coupling scales linearly with the slip-velocity parameter ξ_w, *i.e.*, the prefactor that converts solute gradients into effective hydrodynamic surface velocities [63]. Ajdari and Bocquet [111] have shown that for a partial-slip wall the result by Anderson [63] can be generalized to

$$\xi_w = (k_B T/\mu)\, \lambda_w \gamma_w \, (1 + b_w/\lambda_w)\,, \tag{2.1}$$

where slippage is expressed by the slip length b_w; $b_w = 0$ for a no-slip surface and $b_w \to \infty$ for a full-slip surface. Here, we have introduced k_B the Boltzmann constant, T the temperature, μ the dynamic viscosity, λ_w a length scale for the solute-surface interactions, and γ_w a length measuring the solute excess [111]. For smooth surfaces, as we consider here, the value λ_w is left relatively unaffected by changes in θ, but $b_w \propto (1+\cos\theta)^{-2}$ and $\gamma_w \propto \sqrt{1+\cos\theta}$ [107]. This leads to the following leading-order proportionality of the measured speed with θ:

$$V \propto (1 + \cos\theta)^{-3/2}, \tag{2.2}$$

which requires that $b_w/\lambda_w \gg 1$, see also the Appendix for a more in-depth discussion on the osmotic coupling based mechanism. We use this quantitative relationship between propulsion speed and contact angle to fit the experimental data presented in Figure 2.3B. The proportionality factor A, which contains all other contributions to the speed that are slip independent, is 1.84 μm/s. The excellent agreement between data and model further quantitatively corroborates the influence of slip.

To provide additional support to our hypothesis, we test whether the above dependence persists in the presence of salt. Previous experiments employing 2 μm PS spheres showed that even 1 mM salt considerably decreases propulsion speeds [75, 76]. Although speeds for similar H_2O_2 concentration without salt were different above glass, namely around 4 μm/s [76] and 18 μm/s [75], they reduced to 0.45 and 1 μm/s, respectively, in 1 mM salt. In line with these experiments, we find that speeds

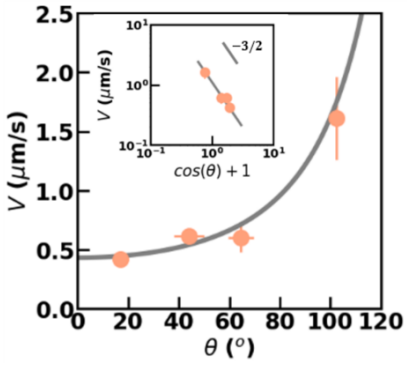

Figure 2.4: **Slip dependence of the propulsion speed V of colloidal swimmers in salt solution.** Speed in 1 mM NaCl as a function of the contact angle θ and least squares fit (solid line) with $V = A(\cos\theta + 1)^{-3/2}$ that follows from our model. The inset shows the data on a log-log scale.

above different substrates decrease with added salt, see Figure 2.4. More importantly, we observe that speeds still follow the same slip dependence. In salt solution, the proportionality factor A is 1.2 μm/s, showing a 33% decrease compared to the salt-free case. Considering that the influence of salt is complex, potentially affecting zeta potentials, separation, higher-order hydrodynamic moments or possibly more properties including bulk speeds, this decrease is not surprising. However, that the same dependence persists further supports the importance of slip, and may provide additional insights into the propulsion mechanism [75].

We emphasize that other substrate properties besides slip may affect propulsion speeds. As mentioned earlier, lowering the substrate zeta potential has been proposed to increase speeds [105]. For completeness we thus measured substrate zeta potentials using a Surface Zeta Potential Cell from Malvern by laser Doppler electrophoresis following Ref. [135] using tracers prepared as in [136], see Methods. We find zeta potentials of -38.3 $\pm$ 1.1 mV and -22 $\pm$ 0.9 mV for glass and PDMS, respectively, in line with this proposal. However, we find an even lower zeta potential, -11 $\pm$ 5 mV, for hydrophilic PDMS. Due to the low speed on hydrophilic PDMS, we conclude that the substrate zeta potential is, surprisingly, not the dominant effect. Secondly, an increase in the substrate roughness was shown to increase the speed [105]. We thus performed Atomic Force Microscopy (AFM) measurements, see Methods. The average substrate roughness Ra, is 1.5 and 5 nm, for glass and PDMS, respectively; with Ra denoting the arithmetic mean of the deviations in height from the roughness mean value. However, hydrophilic PDMS, with a roughness equal or higher [137] to untreated PDMS, featured lower speeds. We thus conclude that substrate roughness is also not the dominant effect here.

Our experiments also provide a new perspective on previous work: the speed increase previously observed on Au-coated surfaces [105] may be due to increased surface slip, since contact angles on Au are typically higher than on glass [138, 139]. Similarly, the speed decrease in [103] may be due to the hydrophilic polyelectrolyte coatings employed on the glass. Besides, our findings may explain the discrepancies in reported speeds between previous experiments. Even though glass substrates were used in all cases, glass can differ in composition, homogeneity and hydrophilicity due to different preparation, coatings, treatment and cleaning methods from the supplier or the researchers themselves, as we have also demonstrated. We also found that contact angles sometimes varied by 10^o within the same type of and/or different parts of the same substrate. AFM indicated that this is likely due to inhomogeneous application or even local absence of coatings applied by the supplier. If the coating or substrate treatment is inhomogeneous or unstable, for example due to a chemical reaction with H_2O_2, a locally or temporally different substrate slip can be observed. For example, we found a 15^o increase in contact angle for the PS substrate before and after being exposed to H_2O_2 for several hours.

Conclusions

Our work points out that nearby walls, though often unconsidered, can significantly impact catalytic microswimmer speeds. Specifically, we find that propulsion speed near a wall is influenced by the wall slip boundary condition. This quantitatively follows from theoretical predictions on the basis of an osmotic coupling mechanism, indicating further control and understanding of the behavior of self-propelled particles. In future work, it would be interesting to investigate if slip affects other features of active motion as well, such as the orientation of active particles with respect to the wall [140]. The here discussed slip dependence of the propulsion speed should not only be relevant for catalytic swimmers but any microswimmer that creates a fluid flow in the vicinity of a substrate.

Acknowledgements

I am grateful to our collaborator Joost de Graaf for developing the osmotic coupling-based mechanism presented here and for much useful discussions. I gratefully acknowledge Rachel Doherty for providing the TPM spheres as well as for help with AFM measurements, contact angle measurements, and substrate functionalizations. I thank Malvern for providing the Surface Zeta Potential Cell and particularly Sandra Remijn for discussions and help with substrate zeta potential measurements. I thank Federica Galli for showing me how to use the AFM, for assisting with AFM measurements and for helpful discussions. I thank Nikos Oikonomeas and Ruben Verweij for help with python routines.

Methods

Synthesis of TPM colloids. Carboxylated 3-(trimethoxysilyl)propyl methacrylate (TPM) spheres with diameter 2.7 μm and polydispersity in size 2.37% were prepared following a one-pot surfactant-free synthesis protocol extended from Ref. [108]. In short, itaconic acid (ITA, Sigma Aldrich) was weighed into a plastic beaker. 30g of MilliQ water (18.2 MΩ cm resistivity, obtained using a Millipore Filtration System Milli-Q Gradient A10) was added and the pH was adjusted to 10.8 with NH_3 (28-30%). The solution was stirred at 300 rpm until ITA was fully dissolved. 900 μL TPM oil (Sigma Aldrich, 98%) was rapidly injected into the stirred solution, which was then covered with parafilm. After 4 h, 100 mg azobis(isobutyronitrile) (AIBN, Sigma Aldrich, $\geq$ 98%) was added. In total the emulsion was stirred for 5 h prior to heating in an oil bath at 80 ^{o}C under rotation at 50 rpm for 2.5 h. The colloids were washed and stored in MilliQ. The resulting spheres have a zeta potential of -70 $\pm$ 2 mV in MilliQ (pH 5.5). Their density is 1.31 kg/L [108].

Preparation of Pt/TPM colloids. TPM spheres were spin coated from ethanol on glass slides at sub-monolayer concentrations and subsequently sputter coated from above with a 4.9 nm Pt/Pd (80/20, MicrotoNano70-PPS708) layer via physical vapor deposition using a standard sputter coating system (Cressington 208HR High Resolution Sputter Coater). During deposition, the stage was rotated at a constant speed to ensure even Pt distribution. The Pt/TPM colloids were redispersed in 5 mM NaOH by 5

min sonication and were subsequently washed and stored in MilliQ water. This method produced single particles. The Pt/TPM spheres have a zeta potential of -55 $\pm$ 2 mV in MilliQ water.

Substrate preparation. *Glass* substrates were purchased from VWR (631-1584 25mm No1) and were used as received unless stated otherwise. They were made of borosilicate glass and were subsequently coated with a Schott's D263M coating by the supplier. According to the supplier, these cover glasses are more hydrophobic than typical soda lime glasses. The measured contact angle for 10% H_2O_2 is $44^o \pm 9^o$. *Hydrophilic glass* was prepared by sonicating the glass substrates for 20 min in acetone, followed by 30 min sonication in ethanol and drying in the oven at 80 ^{o}C for 10 min. The contact angle for 10% H_2O_2 is $30^o \pm 3^o$. *Highly hydrophilic glass* was prepared by immersing the glass substrates in a 1:1 mixture of methanol and hydrogen chloride (37%) for 30 min, followed by thoroughly rinsing with MilliQ water and drying with N_2 [125]. The contact angle for 10% H_2O_2 is $13^o \pm 4^o$. *Hydrophobic glass* was prepared by first immersing glass substrates in 2% Hellmanex while stirring for 30 min. The substrates were then rinsed with MilliQ water and immersed in ethanol for 20 min and dryed in the oven at 150 ^{o}C for 30 min. The dried glasses were then immersed for 20 s in 50 g xylene and 2.9 mL surfasil, for 20 s in xylene and for 60 s in methanol and were dried in the oven at 150 ^{o}C for 30 min. The contact angle for 10% H_2O_2 directly after preparation is $68^o \pm 5^o$. *PDMS* substrates were prepared similarly to [126] using the PDMS kit Sylgard-184 (Dow Corning). The base silicon elastomer and curing agent were mixed at a 5:1 ratio. The mixture was placed in a vacuum desiccator for 1 h to remove trapped bubbles due to agitation, and was then drop casted and flattened on glass. After 45 min in the desiccator, the substrates were dried in the oven at 120 ^{o}C for 3 h. We verified that the contact angle for water on these substrates was 100^o, as stated by the supplier and measured elsewhere [124]; also for 10% H_2O_2, it is $100^o \pm 3^o$. *Hydrophilic PDMS* was prepared by UV-ozone treatment of the PDMS substrates [126, 127] for 60 min using a UVO cleaner (Jelight Company Inc. No 42A-220). This treatment converts the PDMS surface into a silica-like surface, see Ref. [126] for a detailed study on surface properties. The resulting contact angle for water after 60 min treatment was $37^o \pm 7^o$, close to values measured in the literature after similar treatment [127], and indeed close to the contact angle of $30^o \pm 3^o$ that we measured here

for water on clean glass. We note that we perform our experiments within 1 h after surface treatment during which time the substrates remain hydrophilic, see Ref. [127] for the timescale of the hydrophobic recovery of PDMS. *PE* substrates were purchased from ibidi GmbH (μ-slide 8 Well ibiTreat No 80826) and were used as received. These substrates are made from a polyethylene derivative and are subsequently plasma treated by the supplier. The supplier stated that the plasma treatment leads to a permanent change in the substrate properties, however there may be some surface inhomogeneities. The contact angle for 10% H_2O_2 is $51^o \pm 3^o$. *PS* petri-dishes were purchased from Sarstedt and were used as received. The supplier has introduced hydrophilic groups into the surface via a special treatment of the PS. The contact angle for 10% H_2O_2 is $46^o \pm 6^o$.

Imaging and Tracking. TPM/Pt colloids were dispersed in 10% H_2O_2 in MilliQ water at dilute particle concentration ($\approx 10^{-7}$ v/v). Their motion was recorded with a 60x ELWD air objective (NA 0.7) mounted on an inverted Nikon Eclipse Ti microscope. 25 s movies were acquired over the xy plane at 19 frames per second. All measurements were performed in the dark and within the first hour after sample preparation to avoid photocatalytic decomposition of the H_2O_2 [75] and potential changes in the slip of the substrate due to reaction with H_2O_2. At least 70 colloids were imaged and analyzed for all substrates. Additional 30 s movies of the TPM/Pt colloids were taken at 19 frames per second in water, and water containing 1 mM NaCl. Tracking was performed using the python tracking algorithm trackpy that is available online [141].

Data Analysis. The translational diffusion coefficient, D_T, of each TPM/Pt colloid in water above each substrate was extracted by fitting its mean squared displacement (MSD) with $\Delta r^2 = 4D_T\Delta t$, for lag times smaller than 1 s. The diffusion coefficients were then averaged

Substrate	Glass	PDMS	PE	Glass H/ilic	
D_T ($\mu m^2/s$)	0.099	0.105	0.098	0.096	
Error ($\mu m^2/s$)	0.005	0.005	0.008	0.006	
Substrate	PDMS H/ilic	Gl. H/obic	Gl. Highly H/ilic		PS
D_T ($\mu m^2/s$)	0.091	0.098	0.090		0.110
Error ($\mu m^2/s$)	0.003	0.007	0.003		0.003

Table 2.1: Translational diffusion coefficient D_T of the Janus colloids above each substrate in water. The diffusion coefficient D_{bulk} is 0.17 $\mu m^2/s$.

Substrate	Glass	PDMS	PE	Glass H/ilic
Shape	0.68	0.56	1.09	0.45
Location	0.49	0.08	0.71	0.35
Scale	0.87	3.75	0.46	0.52

Substrate	PDMS H/ilic	Gl. H/obic	Gl. Highly H/ilic	PS
Shape	0.67	0.61	0.37	1.03
Location	0.51	0.44	0.22	0.28
Scale	0.26	1.24	0.41	0.87

Table 2.2: Moments of the speed distributions on all substrates as obtained from the log-normal fit.

to obtain the corresponding D_T above each substrate, see Table 2.1 where the reported error is the standard error, calculated from the standard deviation of the corresponding D_T divided by $\sqrt{N-1}$ with N the number of colloids for each substrate. The diffusion coefficient in bulk is 0.17 μm^2/s, obtained from $D_{bulk} = \frac{k_B T}{6\pi\eta\alpha}$. Colloid speeds in the active state were extracted from fitting the first seven data points, corresponding to Δt 0.4 s, of their MSDs in H_2O_2 with the expression

$$\Delta r^2 = 4D\Delta t + V^2\Delta t^2, \tag{2.3}$$

where $\Delta t \ll \tau_R$. Here, τ_R is the characteristic time scale for the particle to undergo rotational diffusion and can be written as $\tau_R = 1/D_{R,bulk}$, with $D_{R,bulk}$ the bulk rotational diffusion coefficient $D_{R,bulk} = \frac{k_B T}{8\pi\eta R^3}$, η the viscosity, k_B the Boltzmann constant, and T the absolute temperature. There is some confusion within the literature concerning Eq. (2.3). Bechinger *et al.* [106] note that this form is incorrect and suggest a factor two should be added to the expression provided by Howse *et al.* [30], *i.e.*, the form provided in Eq. (2.3). The reason for this confusion lies in the fact that Ref. [30] reports a 2D projected MSD for active Brownian particles. Equation (13) from Bechinger *et al.* [106], which provides the full MSD for arbitrary Δt, is instead derived for in-plane motion and rotation of the swimmer *only* about the out-of-plane axis. However, there is a subsequent typo in Ref. [106], which leads to a superfluous factor of 2 in their equivalent of Eq. (2.3), as can be readily seen by taking the Taylor series of their Eq. (13). The short-time diffusion expression by Howse *et al.* [30] is thus internally consistent. Moreover, it coincides with the expression that the authors of Ref. [106] should have obtained for their short-time dynam-

ics. The route followed by Bechinger *et al.* [106] is more appropriate, as our particles are indeed constrained in their reorientation. Lastly, on this topic, we address a similar observation on the correctness of the Howse *et al.* result made in Ref. [142], where the authors provide yet another form of the MSD and consequently Eq. (2.3). This is because these authors are interested in systems for which the swimmer moves in plane, but is presumably able to have an orientation out of the plane; we are not interested in this scenario here. Generally, care needs to be taken in judging which of the three reported expressions is most applicable to the situation studied experimentally. It would be most appropriate to re-derive these from the applicable underlying microscopic dynamics on a case-by-case basis, as only Bechinger *et al.* [106] provide the relevant equations of motion.

Examples of three individual colloid MSDs above three different substrates are shown in Figure 2.5A. To obtain the speed for each colloid, we first fit all colloid MSDs above a specific substrate with both D and V as open parameters. We then use the averaged D value for the substrate as a fixed parameter to obtain V for each colloid. We note that even though the high frame rate allows us to access the short-time behavior, the long-time behavior — or else, the enhanced diffusion regime — is not recovered from our datasets due to the relatively short duration of our measurement. The speed distributions on the different substrates are asymmetric (tail on the right), see Figure 2.5B as an example of the PDF of speeds obtained from fifty individual colloids on hydrophilic glass. We fit the distributions with a log-normal distribution following Goldstein, Lauga, and collaborators [109]. We first performed a Kolmogorov-Smirnov (K-S) test for the goodness of fit, using the statistics package that is build in Python's scipy. From the obtained p-values and the observed agreement between theoretical fit and data, we concluded that the log normal fits the data adequately well. From the fit we obtain the moments of the distributions, see summary of those values in Table 2.2, which we use to determine parameters of the distributions, such as the standard deviation. Due to the distributions being asymmetrical, the peak corresponds to the most frequent value and is therefore representative of the distributions at hand. We therefore determine the fitted peak position of the speed, which takes into account the full shape of the distribution. The corresponding peak values are plotted in Figure 2.3B. The reported error corresponds to the standard error $\frac{\sigma}{\sqrt{N-1}}$, with σ the standard deviation of the distribu-

tion and N the number of colloids. Finally, we extract the characteristic time scale for rotation τ_R from the velocity autocorrelation function following Ref. [110]. We find no correlation between τ_R and the solution contact angle on the different substrates, see Figure 2.5C. We note that on all substrates a few percent of the particles irreversibly adsorbed, except for the PS and highly hydrophilic glass where about 30% and 80% of the particles adsorbed, respectively. Only speeds from colloids with non-zero speeds are included in the PDFs. Moreover, only colloids that do not interact with other colloids are included in the PDFs, since solute gradients in such case may interact and affect the velocities. In addition, colloids with chiral trajectories are not included in the analysis; such colloids are rarely encountered in our samples. We note that for the salt experiments it is hard to obtain sufficient trajectories because sticking of particles increases considerably for all samples/substrates; moreover, Brownian colloids, which also increase with salt, are excluded. Due to having fewer active particles, we cannot plot speed distributions, and therefore report average velocities from arithmetic means in Figure 2.4. However, the K-S test that we perform on the biggest data set showed that the log-normal distribution in principle still fits the data also in salt.

Surface Zeta Potential. Zeta potential measurements were performed with a Malvern Zetasizer Nano ZS, which measures electrophoretic

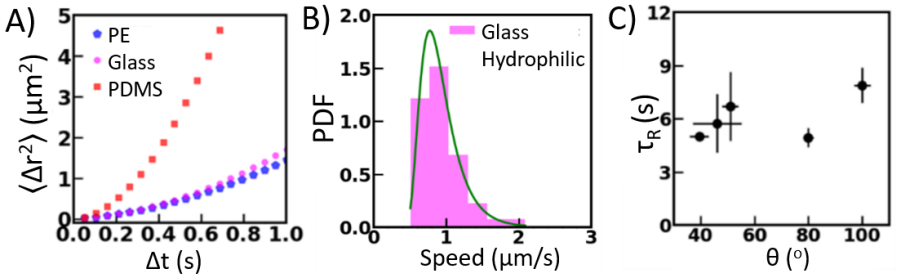

Figure 2.5: A) Typical MSD examples from three individual colloids measured on PE, Glass and PDMS in H_2O_2. B) PDF of colloid speed on hydrophilic glass. The data is fitted with a log-normal distribution. The moments obtained from the fit are shown in Table 2.2. Using these, in addition to the fitted peak position i.e. most frequent speed (0.8 μm/s), we determine the variance (0.078) and standard deviation (0.28 μm/s). C) Averaged τ_R extracted from the decorrelation of the colloid velocity vectors following [110] as a function of contact angle.

mobility of colloidal particles with laser doppler micro-electrophoresis. The zeta potential of the colloids under study was measured in water as well as in acidic pH conditions. In short, we insert a dilute solution of charged colloids in a cell that has an electrode at each end and apply a voltage, causing the colloids to move to the oppositely charged electrode. The resulting phase shifts of the laser light due to the colloid motion are measured by a laser interferometric technique called Phase Analysis Light Scattering, yielding the colloid velocity and electrophoretic mobility. The zeta potential is obtained from the electrophoretic mobility using the Henry equation and the Smoluchowski approximation $\mu = \frac{\epsilon_r \epsilon_0}{\eta}\zeta$, which are incorporated in the Zetasizer.

To measure the substrate zeta potential, the substrates under study were mounted on a planar cell custom made by Malvern for surface measurements. We measured the electrophoretic mobility of charged tracer particles at various distances from the substrate upon applying an electric field. From the tracer electrophoretic mobilities as a function of displacement, the corresponding zeta potentials were obtained through Smoluchowski's equation as a function of displacement and, in turn, the zeta potential at zero displacement (intercept) was extrapolated. The substrate zeta potential was then obtained according to Ref. [135]. Those measurements were performed using 1 μm carboxylated polystyrene colloids as tracers, prepared following a surfactant-free dispersion polymerization protocol, see Ref. [136]. Due to bubble formation at the electrodes in the presence of H_2O_2, all experiments were performed in aqueous HCl. Control experiments for the zeta potential of glass as function of pH (Figure 2.6) were performed in aqueous HCl with pH values equivalent to those at experimental conditions of 0.5-10% H_2O_2. After obtaining good agreement with

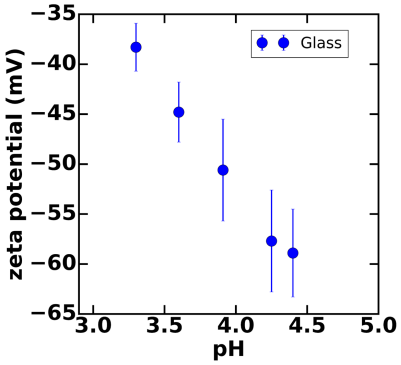

Figure 2.6: **Substrate zeta potential control experiments.** Zeta potential of glass at various acidic pH conditions, in good agreement with streaming zeta potential measurements [143].

streaming zeta potential measurements, we performed the PDMS zeta potential measurements reported in the Results and Discussion section.

Atomic Force Microscopy. Measurements were performed with a JPK Nano Wizard 3 (Ultra Speed) AFM in air, using Opus 240AC-NA probes. The measured frequency and stiffness of the probes were 75 kHz and 1.3 N/m, respectively. Images of the glass and PS substrates were acquired in AC mode, a dynamic contact mode otherwise known as tapping mode. A typical image of a glass substrate used in this work is shown in Figure 2.7: we presume that the spherical nanoparticles seen on the glass are part of the coating applied by the supplier, see Substrate Preparation. A typical image of the PS surface is also shown in Figure 2.7: we presume that the fiber-like surface is either a coating as part of the special treatment that the supplier uses to render the PS hydrophilic, or polishing marks/scratches on the surface to make it flat during the preparation. To avoid harming the surface, images of PDMS were acquired in QI (quantitative imaging) mode, which allows better vertical force control than AC mode and applies no lateral forces on the sample and is thus more suited for softer samples. It is a force curve based mode that provides three dimensional images by measuring the interaction between tip and surface while the tip moves vertically towards the surface, providing an approach and a retract force curve pixel by pixel. From the 3-dimensional images and height profiles, the Ra roughness was directly extracted using the JPK data-processing software version 6.1. The Ra roughness values for glass and PDMS are found under the Results and Discussion section. The Ra roughness for PS is 2.5 nm. The Ra is defined as the arithmetic mean of the deviations in height from the roughness mean value and is given by $Ra = \frac{1}{n}\sum_{i=1}^{n}|y_i|$, where y is the vertical distance from the mean. In air

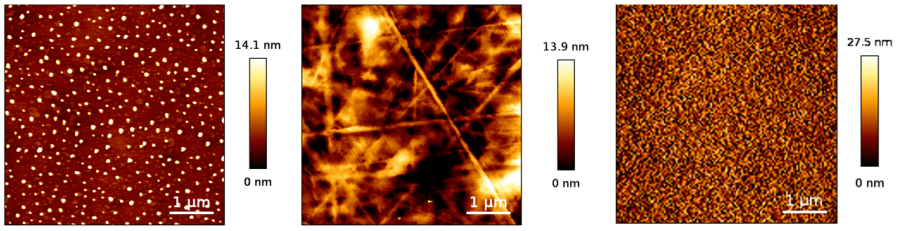

Figure 2.7: From left to right: representative AFM images of the glass, PS and PDMS substrates under study.

and with the same probe we observed from the shape of the approach curves that the stiffness increases from PDMS to glass. However, the stiffness of the PDMS should not be affected by the surface treatment that yields it hydrophilic. Thus, if substrate stiffness affected colloid speeds, speeds on PDMS and hydrophilic PDMS would not be as different.

Contact Angle Measurements. Images were taken with a Canon EF-S 60mm f/2.8 Macro USM lens mounted on a Canon EOS 500D Digital SLR Camera with back-lighting. Water droplets with volumes between 1 and 10 µL were placed on the various substrates. To determine the variation of contact angle for a specific surface, multiple droplets were imaged on the surface. To determine the spread in the contact angle for a certain material, droplets were imaged on different surfaces. These processes were repeated also for droplets containing 10% H_2O_2, 1 mM NaCl, and 10% H_2O_2 with 1 mM NaCl. All images were taken within seconds after droplet placement. The static contact angles were determined using ImageJ. The contact angle for a specific drop is typically determined with an error of less than 1^o. Values reported in Figure 2.3B and under Substrate Preparation, correspond to averaged values from several individual water droplets containing 10% H_2O_2. Values reported in Figure 2.4 correspond to water droplets containing 10% H_2O_2 with 1 mM NaCl. Corresponding errors always denote standard deviations.

Appendix: Mechanism for osmotic coupling-induced speed variation

Understanding the effect of the wetting properties of the wall on the motion of a catalytically propelled swimmer is nontrivial. However, as we will show here, osmotic coupling leads to $V \propto (1+\cos\theta)^{-3/2}$ under certain conditions, thus providing a plausible explanation for our experimental result. We will also discuss other potential mechanisms and explain why these are less likely to account for the significant wall effect.

Relation between slip and contact angle

Before we proceed with our analysis, it is convenient to (re)introduce the concept of slip and contact angle from the Results and Discussion. A hydrodynamic slip boundary condition on a wall (at $z = 0$) is defined as

$$b\frac{\partial}{\partial z}\boldsymbol{u}_i(x, y, z = 0) = \boldsymbol{u}_i(x, y, z = 0), \tag{2.4}$$

where z measures distance normal to a wall, and x and y are orthogonal co-planar coordinates. The fluid velocity is given by $\boldsymbol{u}$ and the subscript $i = x, y$ indicates that the boundary condition is applicable to the co-planar components of the flow vector. Finally, b denotes the slip length, which is zero for a no-slip surface and divergent for a full-slip surface. Regardless of the value of b, the fluid velocity normal to the boundary is characterized by a no-penetration condition: $\boldsymbol{u}_z(x, y, z = 0) = 0$. We do not consider patterned surfaces here, in line with our AFM measurements of the experimental surfaces, see Methods, which means that we can use a single slip value that is homogeneous along the surface.

Huang *et al.* [107] have argued that the following quasi-universal relation between slip b and contact angle θ holds:

$$b \propto (1+\cos\theta)^{-2}, \tag{2.5}$$

where θ is the angle between the surface and a wetting droplet of water in air. The no-slip condition is implied to hold at $\theta = 0$, and the prefactors of the proportionality may be appropriately chosen to achieve this [107].

Diffusion coefficient near surfaces

The surface-to-surface separation between the colloid and the wall δ is important for hydrodynamic and chemical coupling. We therefore analyze its value in this section. It is natural to think that a variation in swim speed stemming from modifying the wall properties may be caused by associated height variations. Such a height change could be a secondary effect of changing the wall's chemical properties, for instance, through changing the electrostatic repulsion. However, it will turn out that this idea does not match with our experimental results.

We find that the separation δ is comparable to the particle radius R. We gain this insight from the experimentally measured diffusion coefficient of our Pt-coated particles in water, see Methods for experimental details and values. The diffusion coefficients are similar within error above all substrates and therefore similarly different from the diffusion coefficient for free diffusion in the bulk. Our results are in agreement with predictions, see for example Ref. [128], on the hydrodynamic mobility of a passive particle moving close to a no-slip wall. We refer to Faxen's theoretical prediction for the near-wall in the plane parallel to the wall diffusion, which has been experimentally proven in Ref. [129] and [130], and is given by $\frac{D}{D_{bulk}} = 1 - \frac{9}{16}\gamma + \frac{1}{8}\gamma^3 - \frac{45}{256}\gamma^4 - \frac{1}{16}\gamma^5$ with $\gamma = R/(\delta + R)$. Faxen's law applies to a no-slip condition, however we are still probing here small departures in terms of slip from this condition. The contact angles that we measure are in the range between 15^o and 100^o, implying that the corresponding slip lengths, calculated by Eq. 2.5, change by roughly a factor of 5. The measured translational diffusion coefficients remain constant upon a variation in slip of that order, and show a reduction of roughly a factor of 2 compared to free diffusion in bulk. Figure 3.1 in Ref. [123], shows the effect of the slip on the force acting on a translating sphere as function of separation distance; the effect on the diffusion coefficient is directly related to the effect on the force, therefore this figure can be used to gauge the effect of the slip on the diffusion coefficient as function of separation distance. To understand the changes in the distance with slip, we look horizontally in the above-mentioned figure — for the here constant diffusion coefficient — and read the separation gap size that would correspond to the changes in separation distance based on the conditions that follow from our measurements. We conclude that for a factor of 2 reduction compared to the bulk value, in combination with the factor 5

change in slip, the variation in the separation will be minimal. Since diffusion coefficients are similarly reduced, we use the average value above the various substrates and find that the separation δ in the Brownian state corresponds to $\delta \sim 0.4R$. Overall, the measured constancy of the passive diffusion coefficients with θ is an indicator that there is limited variation in δ with changes to the wall properties.

Osmotic coupling mechanism

Osmotic coupling can directly affect the speed upon changing the wall, even for fixed δ. We here focus on this mechanism and discuss how such a coupling may give rise to the observed trend. We assume, for convenience, neutral self-diffusiophoresis and homogeneous surface properties for both the wall and the colloid. The properties of the wall and swimmer may be different and we will distinguish these by subscripts w and s, respectively. The discussion is analogous for self-electrophoretic mechanisms, with the minor exception that the Debye length is typically considerably larger than the one associated with non-electrostatic molecular interactions.

Uspal *et al.* [95] have investigated osmotic coupling near a no-slip wall. However, adopting their result is not entirely trivial, as the derivation therein makes explicit use of the fundamental hydrodynamic solutions near a no-slip wall. It is relatively straightforward to compute the Stokeslet for a full-slip wall [144]. However, this limit is problematic for other reasons, as ξ_w will turn out to diverge due to its dependence on θ. The expressions for the Greens functions near a wall with intermediate slip values are convoluted [145] and do not provide significant additional insight beyond what can be obtained through scaling arguments.

Referencing [95], we observe that the osmotic contribution to the speed $\propto (R+\delta)^{-3}$ for no-slip surfaces; this scaling will hold even for partial or full slip. Thus, we may write

$$V \approx V_{other} + \frac{R^3}{(R+\delta)^3} V_{osm.}, \tag{2.6}$$

where $V_{osm.}$ is a proportionality constant that measures the impact of osmotic flow along the wall on the speed of the swimmer above it. The

velocity V_{other} accounts for confinement effects and is here assumed constant with variation of θ, because the height is assumed constant. Both V_{other} and $V_{osm.}$ depend on R, however, only $V_{osm.}$ is strongly dependent on θ. Applying the standard diffusiophoretic theory [63], we have that $V_{osm.} \propto \xi_w / D_{sol.}$ with $D_{sol.}$ the solute diffusion coefficient. Ajdari and Bocquet [111] have shown that for a partial-slip wall the coupling parameter may be written as Eq. (2.1), i.e. $\xi_w = (k_B T/\mu)\, \lambda_w \gamma_w\, (1 + b_w/\lambda_w)$, with k_B the Boltzmann constant, T the temperature, λ_w a length scale for the solute-surface interactions, γ_w a length measuring the solute excess, and b_w the hydrodynamic slip length of the wall. This expression reduces to the no-slip result for $b_w = 0$. Note that typically $b_w \gg \lambda_w, \gamma_w$ [111], implying that the dominant effect of changing the wall comes from the hydrodynamic slip this induces. The value λ_w is left relatively unaffected by changes in the wall, as the interaction length scale is molecular ≈ 1 Å for neutral solutes. However, γ_w will vary as it depends on details of the molecular interactions between solutes and wall, which are key to determining wetting (and slip). Following Huang *et al.* [107], we have

$$\gamma_w \propto \sqrt{1 + \cos\theta}, \tag{2.7}$$

and for b_w we can use Eq. (2.5). Isolating the dominant dependence on θ, we obtain the following proportionality

$$V \propto V_{osm.} \propto \frac{1}{(1 + \cos\theta)^{3/2}}, \tag{2.8}$$

whenever $b_w \gg \lambda_w, \gamma_w$, such that the slip-length term dominates.

Implications of the mechanism and other considerations

Equation (2.8) has some interesting consequences and caveats in relation to our experimental data. First, the presence of the factor 1 in the numerator to Eq. (2.8) allowed us to capture the finite (extrapolated) speed at $\theta = 0$ and the global trend well, without requiring an offset to Eq. 2.8. That is, a nearly negligible offset best fits the data. The implication is that the prefactors and separation δ in Eq. (2.6) are such that for a no-slip surface there is some (fortuitous) cancellation of terms that eliminate the

V_{other} contribution to the speed. This could be an expression of a competition between confinement, bulk, and osmotic effects, which may have opposite signs. It is difficult to make strong statements in this regard without knowing more about the specifics of the propulsion mechanism.

A most interesting feature of Eq. (2.8) is the potential for a divergence of the speed of a self-propelled particle near a full-slip surface. This is counter intuitive as for a dragged passive sphere the mobility enhancement with respect to bulk is only a factor 1.37 [123, 146] in the full-slip case. The reason for this is that the surface velocity generated by the osmotic coupling can become very significant, as there is a divergent separation in length scales between the atomic interactions that force the fluid λ_w and the hydrodynamic slip length b_w as θ approaches $180°$. Such a divergence does not occur in a real system as the effect of enhanced surface speed would either push the solute concentration out of the low-Péclet regime where solute diffusion dominates its advection by the fluid, or modulate the swimmer height; both effects being self-limiting in nature.

Lastly, we discuss other arguments for describing our findings, such as purely hydrodynamic coupling and solute-species confinement. By purely hydrodynamic coupling we mean the modification of the (bulk) flow field around the swimmer through the presence of the wall, but in absence of the osmotic effect. This type of coupling has been investigated in detail for simple swimmer models, *e.g.*, see Ref. [132]. Flow-mediated interactions give rise to attraction and repulsion for pusher and puller swimmers, respectively, and may also lead to swimmer reorientation [102, 132, 133]. At a constant, yet small value of $\delta \lesssim R$, hydrodynamic slip can modify the mobility of a passive particle substantially [123, 146]. However, a purely hydrodynamic effect is unlikely to describe our experiment, because at a fixed δ boundaries perturb the parallel motion of an active particle less than that of a passive one. The former has a leading-order dipolar flow-field decay [132], while the latter has a leading-order monopolar decay, explaining the difference. It is straightforward to demonstrate that within far-field theory the effect is less than 10% of the bulk speed for a squirmer-type swimmer [147, 148] moving parallel to the wall, even for small δ. We also consider solute-species confinement in the gap between wall and swimmer, which perturbs concentration gradients along the colloid surface, affecting the colloid slip velocity and thus its speed; this effect

comes on top of any purely hydrodynamic change of the velocity. This coupling has already been studied [96, 97, 99–101]. Yet, under the fixed height assumption the effect of this mechanism should be limited. This is because the Péclet number typically is small and the solute species are not substantially impacted by changes in the hydrodynamic flow field, due to wall modification. Considering the above, we believe that the osmotic coupling scenario is the most likely candidate for describing our observations.